

# Open Stamped Parts Dataset\*

Sarah Antiles<sup>1</sup> and Sachin Talathi<sup>2</sup>

**Abstract**—We present the Open Stamped Parts Dataset (OSPD), featuring synthetic and real images of stamped metal sheets for auto manufacturing. The real part images, captured from 7 cameras, consist of 7,980 unlabeled images and 1,680 labeled images. In addition, we have compiled a defect dataset by overlaying synthetically generated masks on 10% of the holes. The synthetic dataset replicates the real manufacturing environment in terms of lighting and part placement relative to the cameras. The synthetic data includes 7,980 training images, 1,680 validation images and 1,680 test images, each with bounding box and segmentation mask annotations around all holes. 10% of the holes in the synthetic data mimic defects generated in the real image dataset. We trained a hole-detection model on the synthetic-OSPD, achieving a modified recall score of 67.2% and a precision of 94.4%. We anticipate researchers in the auto manufacturing and broader machine learning and computer vision communities using OSPD to advance the state of the art in defect detection of stamped holes in the metal-sheet stamping process. The dataset is available for download at: <https://tinyurl.com/hm6xatd7>.

## I. INTRODUCTION

In auto manufacturing, sheet metal stamping is a cost-effective way to shape and cut flat metal sheets to produce several customized components of the vehicle at high-volume [1]. Sheet metal stamping is a complex process where precise design and tooling is required to minimize defects and ensure optimal part quality. A multitude of defects, while rare, may still occur during production including but not limited to, splits [2], imprints [3] and missing stamped holes.

Manual inspection of stamped parts is time-consuming and susceptible to human errors. During this process, inspectors remove sheets from the production line to individually check defects, for example, missing stamped holes, a laborious task due to the numerous, sometimes very small, holes. Consequently, manual inspection of every sheet is impractical. The high cost of manual inspection coupled with the costly consequence of defects, have spurred research interest in automated defect detection systems. Automation promises increased reliability, scalability, and cost-effectiveness.

In manufacturing, machine vision is increasingly used for part inspection. This involves capturing images via optical sensors followed by image processing to extract meaningful information. Processing techniques range from more traditional computer vision approaches to more advanced deep learning approaches. Because auto manufacturing settings are particularly dynamic, deep learning techniques, which learn pertinent information from the data, are advantageous [2].

\*This work was supported by General Motors

<sup>1</sup>Sarah Antiles is with General Motors, primary contributor [sarah.antiles@gm.com](mailto:sarah.antiles@gm.com)

<sup>2</sup>Sachin Talathi is with General Motors, senior author [sachin.talathi@gm.com](mailto:sachin.talathi@gm.com)



Fig. 1: a. Example of synthetically rendered stamped metal sheet b. Example of real stamped sheet metal on conveyor belt in factory setting.

Deep learning spans various tasks including image classification, object detection, semantic segmentation, and instance segmentation. Our focus is on object detection because we require real-time localization and classification of defects, which we treat as individual objects.

The lack of publicly available training data poses a challenge for leveraging deep learning to develop models for sheet metal defect detection. Common object detection models such as YOLO [4] and Faster R-CNN [5] are often trained on datasets like ImageNet [6] and COCO [7], which belong to the category of natural images and are distinctly different from images of sheet metal captured in an industrial setting.

Addressing the data challenge could involve training object detection models using synthetically generated images. Still, replicating the manufacturing environment proves difficult, often leading to a domain gap between synthetic and real data [8]. In our dataset, one such gap lies in the background of the stamped sheet: synthetic images feature empty backgrounds, while real images depict conveyors and wire meshes. Refer to Fig. 1 for a visual representation of this domain gap in our data. Recent strides in generative deep learning techniques offer promise in minimizing this gap, enhancing the robustness of object detection solutions [9], [10].

In order to facilitate these types of investigations, our work is focused on compiling a dataset of real sheet metal parts coupled with a large set of labeled synthetic sheet metal parts. We also develop a baseline hole detection model and present model performance numbers in terms of modified-recall and precision scores, specifically designed to evaluate the potential utility of the model when deployed on the factory floor.

Our hope is that the proposed baseline model, evaluation

metrics, and datasets (both real and synthetic) of sheet metal images, the Open Stamped Parts Dataset (OSPD), will facilitate further development of efficient and reliable machine vision models to automate the process of defect inspection in auto manufacturing.

Our key contributions are summarized as follows:

- A labeled set of grayscale real images with bounding box annotations<sup>1,2,3</sup>.
- A labeled set of grayscale real images with simulated missing hole defects and bounding box annotations<sup>1,2,3,4</sup>.
- A large scale, labeled synthetic dataset to mimic the real data with segmentation masks and bounding boxes<sup>1,3,5</sup>.
- A large scale, unlabeled set of real images<sup>1</sup>.
- Model benchmarks for hole detection on stamped metal parts using state-of-art deep learning techniques for real-time inspections.
- Modified recall metric for evaluating models based on desire to penalize defects resulting from stamping error.

## II. RELATED WORK

### A. Inspection of Stamped Parts in Auto Manufacturing

Singh *et. al* introduce a YOLO variant trained on High Dynamic Range (HDR) photos to identify neck and split defects on sheet metal [2]. Guo *et. al* present an approach tailored for manufacturing, utilizing solely unlabeled real images to detect metal artifacts [11]. In our research, we incorporate unlabeled images for training, augmenting them with labels obtained from synthetic data. Block *et. al* employ RetinaNet to detect metal part defects, later employing the MOSSE tracker algorithm to correlate detections over time, effectively mitigating false positives [3]. False positives, which we define as the detection of a hole which does not exist, pose a significant concern in our context if the hole category deemed as found is in fact missing. Further details regarding our false positive reduction filtering method are elaborated on in the *Model Description* section.

### B. Surface Inspection Datasets

In Huang *et. al*, 1,386 images of circuit boards with 6 types of defects are labeled for detection, classification, and registration tasks [12]. Real circuit boards are augmented with a synthetic defect generated with Adobe® Photoshop® software. One defect category, the “missing hole”, presents itself as a ring-like artifact with uniform green background.

<sup>1</sup>Metadata includes camera name and trigger distance.

<sup>2</sup>See Fig. 2 for diagram of camera fixture. Trigger distance (measured in millimeters) measures the distance the sheet metal has travelled along the conveyor relative to the fixture entrance.

<sup>3</sup>Metadata includes whether or not the hole is graded. A graded hole is defined as one where all edges of the hole are visible in the reference image and the hole size is 100 pixels or larger. A reference image is a single real image for each camera and trigger distance combination (also referred to as a “view”) where there is neither sheet metal part shift relative to the camera nor camera shift relative to its expected position.

<sup>4</sup>Metadata includes whether or not the hole is masked.

<sup>5</sup>Metadata includes the angle between the relative normal of the hole center and the camera.

TABLE I: Public Surface Inspection Datasets

Dataset	Image Type	#Images	Task	Synth. / Real
PCB [12]	HDR RGB	1,386	Classification Detection Registration	Synth.
Severstal [13]	grayscale	18,074	Semantic Segmentation	Real
DAGM [14]	grayscale	16,100	Detection	Synth.
NEU [15]	grayscale	1,800	Detection	Real
OSPD	grayscale	11,340	Detection Instance Segmentation	Synth.
OSPD	grayscale	9,660	Detection	Real

In contrast, the OSPD missing hole defect may not be distinguishable from the rest of the metal sheet. Thus, the focus in OSPD is to detect existing holes, which exhibit highly variable texture largely consisting of the background behind the stamped metal sheet.

Other datasets include 18,074 images of flat steel sheets with four labeled defect types [13], 16,100 images of synthetically generated textured surfaces designed for industrial optical inspection with the defect labeled at the image level [14], and 1,800 images of real steel surface inspections with 6 labeled defect types [15]. Unlike these datasets where the object of interest is on the metal surface itself, in OSPD, the object of interest is the stamped hole. A further comparison of these datasets to the OSPD can be found in Table I.

### C. Transfer Learning Between Synthetic and Real Data

When a new part is onboarded, little to no real data is available for training a neural network. Training on synthetically generated data becomes imperative in these scenarios, and several works aim to bridge the gap between the real and synthetic data through different techniques [9] [10]. See the *Experiments* section for a performance comparison of models trained on synthetic data that has and has not been transformed by an image-to-image translation model.

## III. DATA COLLECTION PROCESS

### A. Camera Fixture Setup

The OSPD’s image collection involves a camera fixture equipped with 10 cameras positioned across its left, right, entrance, and exit sides, totaling 40 cameras. Entrance/exit designations are relative to conveyor belt movement, while right/left designations are relative to viewing from the entrance side. Each camera is named “ZxCAMy,” where  $x=1$  and  $x=2$  specify left and right-side camera respectively and  $y \in [1,20]$ . Refer to Fig. 2 for a diagram illustrating the fixture, annotated with camera names. In the OSPD, images are exclusively sourced from a subset of left-sided

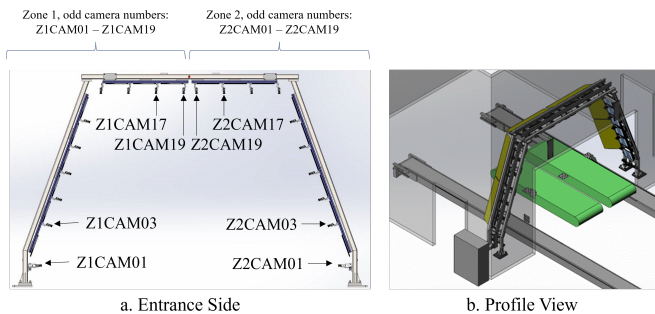


Fig. 2: a. Subset of cameras labeled on fixture’s entrance side. Exit side mirrors entrance side, but with even-numbered cameras b. Illustration of conveyor passing through fixture.

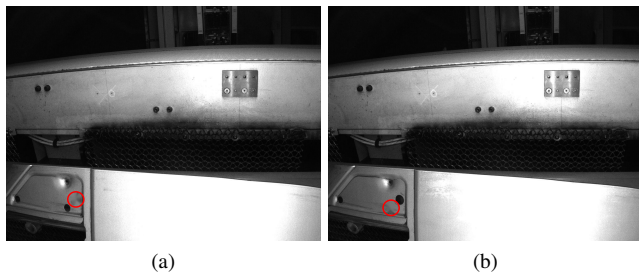


Fig. 3: Examples of masked holes. a. Hole category, DY1, outlined in red as masked b. Hole category, DY2, outlined in red as masked.

cameras. Each camera may trigger multiple times at varying distances as the part moves through the fixture. In OSPD, the COCO-formatted metadata for each image includes the camera name and trigger distance within the “cam\_name” and “trigger\_mm” fields, respectively. Lights on the fixture are infrared and cameras have infrared filters installed on their lens’ to block out other light sources.

### B. Data Generation and Acquisition

The synthetic data was acquired using Unreal Engine [16], by carefully configuring parameters such as camera angle, focal length, and lighting to replicate the actual production environment. The simulation generated images of a stamped sheet with 7 distinct hole categories. To mimic missing stamped-hole defects, we applied a mask to a hole in any image with 10% probability. It’s important to note that the conveyor and other background elements present in the manufacturing facility were not generated in Unreal Engine, resulting in a domain gap between synthetic and real data, which we aim to address.

The real data used for testing was taken over the course of two days in March and April, 2023. To assess a model’s ability to identify missing holes accurately, while lacking actual instances of missing holes in real data, we transformed the test dataset by applying masks to a subset of the holes using an inpainting technique [17]. Refer to figure 3 for representations of two different masked holes.

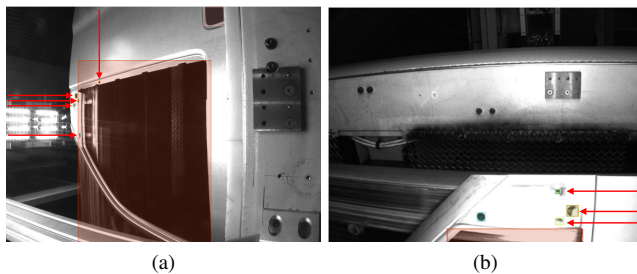


Fig. 4: Examples of labeled hole images. Each hole is enclosed in a bounding box colored according to its category ID. Arrows point to the referenced hole annotations a. Small holes, difficult to detect by the human eye, were labeled b. Partially visible, low contrast holes were labeled.

We randomly assigned a mask to each hole in the real data with 10% probability, resulting in 665 masked holes while the synthetic data has 4,964 masked holes. Because holes were masked at random, the percentages of masked holes in synthetic versus real data are comparable, though not identical.

The unlabeled real data was collected over a period of 12 inspections days in August and September, 2023. Inspections were taken by the same cameras at the same trigger distances as the inspections in the labeled real data. Unlabeled real data is provided in the same quantity as the synthetic training set: there are 380 instances for each of the 21 views for a total of 7,980 images.

### C. Labeling Process

Five individuals manually labeled the stamped holes using Label Studio [18]. To ensure accuracy and consistency, each person’s labels underwent review by two others. Randomized labeling assignments prevented any individual from exclusively labeling all instances of a particular view.

Labelers were instructed to create bounding boxes around entire holes, despite potential difficulties in detection, given prior knowledge that all holes were present during inspections. Examples of challenging-to-detect holes, appropriately annotated, are depicted in Fig 4. For testing purposes, only graded holes were considered. See footnote 3 on page 2 for the definition of a graded hole. Additional details regarding evaluation metrics are available in the *Metric* section.

To create masked holes in the real data, we had a group of six labelers annotate holes with polygon masks in Label Studio. They were instructed to trace the hole’s contour as accurately as they could. Subsequently, each label was reviewed by two other labelers for verification.

## IV. IMAGE SETS & STATISTICS

We provide five datasets:

- 1) **Synthetic:** data generated by Unreal Engine; subset of holes masked; split into train, validation and test sets.
- 2) **Real, labeled, reference:** available for use in training; only graded holes labeled; no masked holes.

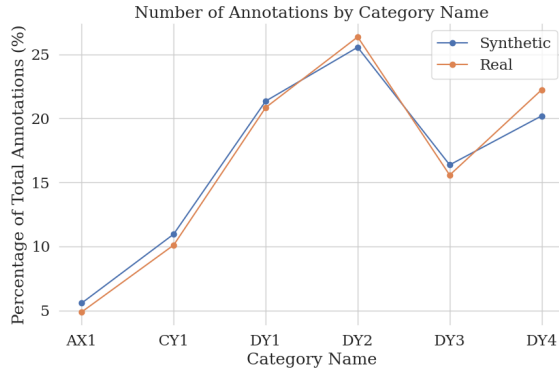


Fig. 5: Number of graded annotations by category for synthetic and real data.

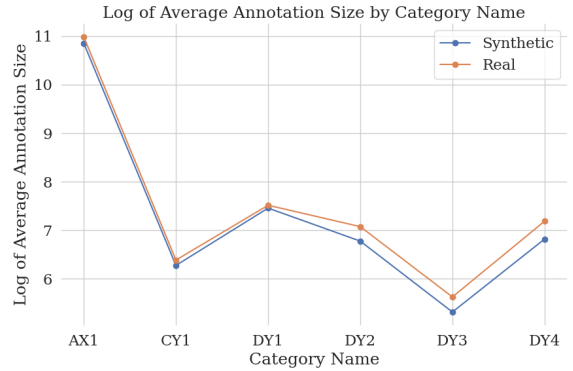


Fig. 6: Average bounding box area in log scale by category for graded annotations in synthetic and real data.

- 3) **Real, unlabeled:** available for use in training; no masked holes.
- 4) **Real, labeled:** dedicated for model testing only; no masked holes.
- 5) **Real, labeled, 10% masked:** dedicated for model testing only; is copy of “real labeled” data with subset of holes masked.

Fig. 5 shows the number of graded holes in the synthetic data and real data for each hole category. While absolute numbers for the synthetic data are larger than those for the real data, the relative quantities of each hole category across synthetic and real are comparable.

Our primary objective is to accurately detect the presence of all holes, and thereby identify any missing ones. In practical production scenarios, the occurrence of a missing hole is extremely rare (<1% chance); however, the consequences of not detecting a missing hole are high.

Considering that neural networks learn from examples, and noting that there are limited instances of missing holes in actual production data, we opted to increase the probability of missing holes in the synthetic training data beyond the expected frequency in real-world scenarios.

Since the recording session used to compile the real dataset didn’t identify any missing holes, we have provided a separate dataset named “real, labeled, 10% masked”, where masked holes are artificially generated. This dataset serves the purpose of evaluating a model’s ability to properly recognize the absence of a hole.

The average size (measured in pixels per inch) of each graded hole, which is calculated as the area of the bounding box, is shown in fig. 6 for both synthetic and real, labeled data. On average, hole category AX1 is significantly larger than the other graded holes. Differences in the distribution of the area of each hole by category between synthetic and real is largely due to part shift relative to the camera, which is simulated in synthetic data and observed in real data. For further detail on number of holes by category and camera view, please refer to supplementary statistics at: <https://tinyurl.com/hm6xatd7>.

Fig. 7 compares the brightness levels across three datasets:

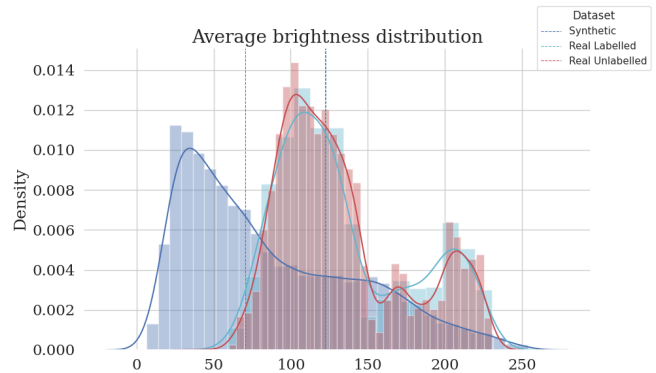


Fig. 7: Average image brightness distributions across datasets. Vertical dotted lines indicate distribution medians.

synthetic, real labeled, and real unlabeled. Notably, relative to the brightness distribution of synthetic data, the brightness distributions of the real unlabeled and real labeled images show a stronger resemblance.

We note that masked holes are undersampled in the data relative to unmasked holes. It is however crucial to highlight that the shape and texture of a missing hole are not well-defined in practical production scenarios. This factor motivates our emphasis on detecting holes rather than specifically targeting the detection of missing holes. For a deeper understanding of how we address this undersampling during the evaluation of our models, please refer to our explanation of modified recall score in the *Metric* section.

Not all hole categories are equally represented across the dataset or across different views. For instance, AX1, the largest graded hole, constitutes only 6% of graded holes in the synthetic data and 5% of graded holes in the real data. Hole BY1, though present, is not graded.

## V. MODEL DESCRIPTION

### A. Object Detection

YOLO, a leading CNN based object detection model serves as our baseline model [4]. Specifically, we train a

YOLOv7 model<sup>1</sup>, as it demonstrates superior speed and accuracy compared to prior YOLO architectures [19].

The YOLOv7 model, starting with pre-trained model weights and p5 hyperparameters, was trained for 1,000 epochs with a batch size of 8 on an NVIDIA A100 GPU. Training images were resized to 640x640, padding the smaller dimension of the original image to maintain the aspect ratio.

For training of the binary hole/no-hole models, we chose to assign categories to predictions through a post-processing step that rests on the assumption that each view has a defined set of expected hole categories given by the view’s reference image. The procedure for filtering predictions and assigning category is as follows:

For each image,  $I$ , in the test set, grab its corresponding reference image,  $R$ , and for each annotation,  $f_r$ , in the reference image, map it to a subset of predictions,  $\{i_p | i_p \subseteq I_p\}$ , where  $I_p$  is the set of model predictions on image,  $I$ . We create this mapping by first considering all predictions as potential matches to the reference annotation and then filtering out predictions through a method as follows:

- 1) If the area of  $f_r$ ,  $a_r$ , is greater than 1,100 pixels, calculate the structural similarity measure (SSIM) [20], average local binary patch (LBP) [21] and template match score (TMS) [22] between the cropped image contained in  $i_p$  and  $f_r$  to obtain:  $SSIM_{i,f}$ ,  $LBP_{i,f}$  and  $TMS_{i,f}$ . Filter out  $i_p$  where  $SSIM_{i,f} < 0.19$ , Keep all  $i_p$  where  $SSIM_{i,f} > 0.45$ , and for  $i_p$  where  $SSIM_{i,f} > 0.19$  and  $SSIM_{i,f} < 0.45$ , do<sup>2</sup>:

- Filter out  $i_p$  where  $LBP_{i,f} > 0.007$
- Filter out  $i_p$  where the  $TMS_{i,f} \leq 0.925$

If  $a_r \leq 1,100$ , filter out all  $i_p$  except for  $i_p$  whose center is nearest to  $f_r$ .<sup>3</sup> After all  $f_r$  have been considered, each  $f_r$  will be assigned to zero, one, or many  $i_p$ .

- 2) Find the maximum cardinality matching by solving the minimum cost assignment algorithm where cost values in our cost matrix are defined as the Manhattan distance between the center of  $i_p$  and  $f_r$  and the boolean matrix is derived from the previous step where we found potential matches [23]. In this way, each  $i_p$  is assigned to at most one  $f_r$  and each  $f_r$  is assigned to at most one  $i_p$  [24].
- 3) Assign category ID to  $i_p$  according to the ID of its assigned  $f_r$ .

Note, step 3 is only used in binary-class models. For multi-class YOLO models, we perform steps 1 and 2 only.

### B. Unpaired Image-to-Image Translation

Image-to-Image (I2I) translation is a specific use case in generative modeling of digital images, where the objective is to synthesize an output image to match the texture and pixel distribution of images in the target domain from images in

the source domain, while preserving the structure and content of the input image [25], [26]. In the context of sheet metal stamping, synthetic images belong to the source domain and the sheet metal images obtained from the factory floor belong to the target domain.

In our I2I experiments, we train a contrastive unpaired translation (CUT) image-to-image translation model using unpaired synthetic and real images [27]. We then feed our synthetic data through this model to realify the data and train a YOLOv7 model.

### C. Metric

Our foremost goal is to accurately identify missing holes; classifying a missing hole as found can significantly compromise this objective. Misclassification can occur in two ways: the model either recognizes a missing hole as a hole or identifies a different object as a hole. Consequently, our metric aims to reflect our strong preference for zero false positives in both of these scenarios. Provided there is a low occurrence of false positives on objects, our secondary objective involves minimizing instances where the model incorrectly labels an existing hole as missing. As such, we define a best model as one with the highest  $F_\beta$  score:

$$F_\beta = (1 + \beta^2) \cdot \frac{\text{precision} \cdot \text{recall}}{\beta^2 \cdot \text{precision} + \text{recall}} \quad (1)$$

where  $\beta = 0.9$ , showing our preference for models with higher precision over higher average modified recall. We define precision in the standard way<sup>4</sup>. “Modified recall” combines the traditional recall calculated on the real, labeled dataset with an additional penalty term for any predictions made on masked holes within the real, labeled 10% masked dataset. The equation for modified recall is as follows:

$$\frac{1}{J} \sum_{j=1}^J r_{u,j} * \frac{e^{-1} f p_{m,j} + t_{m,j} - f p_{m,j}}{t_{m,j}} \quad (2)$$

Here,  $J$  represents the total number of graded hole categories,  $r_{u,j}$  represents the recall calculated on the real, labeled dataset of graded holes for hole category  $j$ ;  $f p_{m,j}$  represents the false positive predictions of hole category  $j$ , made on masked holes (graded or ungraded) within the real, labeled, 10% masked hole dataset; and  $t_{m,j}$  denotes the total number of masked holes in the real, labeled 10% masked hole dataset<sup>4</sup>.

## VI. EXPERIMENTS

Table II displays the confidence threshold, average modified recall, and average precision that yields the highest  $F_{0.9}$  score where confidence threshold was tested at 5% increments from 50% to 95%. Synthetic models are YOLOv7 models trained on data generated directly by Unreal Engine while I2I models are YOLOv7 models trained on data generated by Unreal Engine and then fed through a CUT image-to-image translation model [27]. Multi-class models

<sup>1</sup>Code available at <https://github.com/WongKinYiu/yolov7>

<sup>2</sup>Bounds derived empirically

<sup>3</sup>Manhattan distance is used for calculating distance [23]

<sup>4</sup>Intersection over union threshold is 0.2 if area of ground truth annotation  $< 96^2 = 9,216$ , else, threshold is 0.5.

TABLE II: Model Results

Model	Conf. Thresh.	Avg. Modified Recall	Avg. Precision	F <sub>0.9</sub> Score
Synthetic – multi-class	60	67.2	94.4	79.9
I2I – multi-class	65	58.7	73.1	65.9
Synthetic – binary + custom category ID protocol	75	61.1	81.6	70.9
I2I – binary + custom category ID protocol	65	57.7	86.4	70.7

predict each object as one of several hole classes and are fed through the filtering method outlined in the *Model Description* section for increasing precision. The binary + custom category ID protocol models predict each object under a single hole class and are fed through the protocol outlined in the *Model Description* section for filtering and category assignment. Because we are interested in optimizing the modified recall metric, we chose to evaluate each model using the model checkpoint which yields the highest recall on the validation set during training. Training a multi-class model with purely synthetic data yields the highest modified recall, 67.7, and highest precision, 94.4. I2I appears to add no increase in performance.

## VII. CONCLUSION

We introduced OSPD, a dataset comprising synthetic and real stamped metal sheets, which aims to enhance defect detection of stamped holes in manufacturing. Our custom metric prioritizes identifying missing holes, and we presented a baseline model as a starting point for future enhancements. Finally, our statistical analysis of the data offers contextual insights and identifies potential sources of model bias.

## ACKNOWLEDGMENT

Thank you to Anishi Mehta for her contributions in literature review, editing and planning. Thank you to Rosemary Binny, Sherry Courington, Carlos Cardenas, Beatrice Lovely, Anishi Mehta, Joseph Muniz Jr., and Jose Rangel, who labeled our data. Thank you to Hilton Shumway, Sean Sloan and Anthony Swink who worked with Unreal Engine to generate synthetic data. Thank you to Jose Armando Lopez Jr., Steve Rangos, Thomas Sandrisser, and Tyler Wingo for their review and edits. Thank you to Jose Armando Lopez Jr. and Thomas Sandrisser for their support of this project.

## REFERENCES

- [1] S. Bobade and T. Y. B. Badgujar, "A state of art in a sheet metal stamping forming technology-an overview," *International Journal Of Advance Research And Innovative Ideas In Education*, vol. 3, 01 2017.
- [2] A. Singh, T. Bashford-Rogers, D. Marnerides, K. Debattista, and S. Hazra, "Hdr image-based deep learning approach for automatic detection of split defects on sheet metal stamping parts," *The International Journal of Advanced Manufacturing Technology*, vol. 125, 01 2023.
- [3] S. Block, R. Silva, L. Dorini, and R. Minetto, "Inspection of imprint defects in stamped metal surfaces using deep learning and tracking," *IEEE Transactions on Industrial Electronics*, vol. PP, pp. 1–1, 04 2020.
- [4] J. Redmon, S. Divvala, R. Girshick, and A. Farhadi, "You only look once: Unified, real-time object detection," in *2016 IEEE Conference on Computer Vision and Pattern Recognition (CVPR)*, pp. 779–788, 2016.
- [5] S. Ren, K. He, R. B. Girshick, and J. Sun, "Faster R-CNN: towards real-time object detection with region proposal networks," *CoRR*, vol. abs/1506.01497, 2015.
- [6] J. Deng, W. Dong, R. Socher, L.-J. Li, K. Li, and L. Fei-Fei, "Imagenet: A large-scale hierarchical image database," in *2009 IEEE Conference on Computer Vision and Pattern Recognition*, pp. 248–255, 2009.
- [7] T.-Y. Lin, M. Maire, S. Belongie, L. Bourdev, R. Girshick, J. Hays, P. Perona, D. Ramanan, C. L. Zitnick, and P. Dollár, "Microsoft coco: Common objects in context," 2015.
- [8] J. Tremblay, A. Prakash, D. Acuna, M. Brophy, V. Jampani, C. Anil, T. To, E. Cameracci, S. Boochoon, and S. Birchfield, "Training deep networks with synthetic data: Bridging the reality gap by domain randomization," 2018.
- [9] J. Wang, T. Shen, Y. Tian, W. Yutong, C. Gou, X. Wang, F. Yao, and C. Sun, "A parallel teacher for synthetic-to-real domain adaptation of traffic object detection," *IEEE Transactions on Intelligent Vehicles*, vol. 7, pp. 1–15, 09 2022.
- [10] A. Petsiuk, H. Singh, H. Dhadwal, and J. M. Pearce, "Synthetic-to-real composite semantic segmentation in additive manufacturing," 2022.
- [11] S. Guo, D. Wang, Z. Feng, and W. Guo, "Uir-net: Object detection in infrared imaging of thermomechanical processes in automotive manufacturing," *IEEE Transactions on Automation Science and Engineering*, vol. PP, pp. 1–12, 10 2021.
- [12] W. Huang and P. Wei, "A pcb dataset for defects detection and classification," 2019.
- [13] A. Grishin, BorisV, iBardintsev, inversion, and Oleg, "Severstal: Steel defect detection." <https://kaggle.com/competitions/severstal-steel-defect-detection>, 2019.
- [14] F. H. M. Wieler, T. Hahn, "Weakly supervised learning for industrial optical inspection." <https://doi.org/10.5281/zenodo.8086136>, DAGM 2007.
- [15] K. Song and Y. Yan, "A noise robust method based on completed local binary patterns for hot-rolled steel strip surface defects," *Applied Surface Science*, vol. 285, pp. 858–864, 2013.
- [16] Epic Games, "Unreal engine."
- [17] A. Telea, "An image inpainting technique based on the fast marching method," *Journal of Graphics Tools*, vol. 9, 01 2004.
- [18] M. Tkachenko, M. Malyuk, A. Holmanyuk, and N. Liubimov, "Label Studio: Data labeling software," 2020-2022. Open source software available from <https://github.com/heartexlabs/label-studio>.
- [19] C.-Y. Wang, A. Bochkovskiy, and H.-Y. M. Liao, "Yolov7: Trainable bag-of-freebies sets new state-of-the-art for real-time object detectors," 2022.
- [20] Z. Wang, A. Bovik, H. Sheikh, and E. Simoncelli, "Image quality assessment: from error visibility to structural similarity," *IEEE Transactions on Image Processing*, vol. 13, no. 4, pp. 600–612, 2004.
- [21] L. Liu, P. Fieguth, Y. Guo, X. Wang, and M. Pietikäinen, "Local binary features for texture classification: Taxonomy and experimental study," *Pattern Recognition*, vol. 62, pp. 135–160, 2017.
- [22] J. Lewis, "Fast normalized cross-correlation," *Ind. Light Magic*, vol. 10, 10 2001.
- [23] M. D. Malkauthekar, "Analysis of euclidean distance and manhattan distance measure in face recognition," in *Third International Conference on Computational Intelligence and Information Technology (CIIT 2013)*, pp. 503–507, 2013.
- [24] L. Ramshaw and R. E. Tarjan, "On minimum-cost assignments in unbalanced bipartite graphs," 2012.
- [25] Y. Pang, J. Lin, T. Qin, and Z. Chen, "Image-to-image translation: Methods and applications," *IEEE Transactions on Multimedia*, vol. 24, pp. 3859–3881, 2022.
- [26] A. Alotaibi, "Deep generative adversarial networks for image-to-image translation: A review," *Symmetry*, vol. 12, no. 10, 2020.
- [27] T. Park, A. A. Efros, R. Zhang, and J.-Y. Zhu, "Contrastive learning for unpaired image-to-image translation," 2020.